Translating clean liquid fuels synthesis with low aromatics over NaFe@C/ HZSM-22 directly in CO_2 hydrogenation

Cederick Cyril Amoo [a,b], Joshua Iseoluwa Orege [a,b], Qingjie Ge [a,*], Jian Sun [a,*]

[a] *Dalian National Laboratory for Clean Energy, Dalian Institute of Chemical Physics, Chinese Academy of Sciences, Dalian 116023, China*
[b] *University of Chinese Academy of Sciences, Beijing 100049, China*

ARTICLE INFO

ABSTRACT

Fuel production is an option for valorizing CO_2, yet deficient catalysts meeting the standard fuel production has impeded progress of this promising technology. Herein, liquid fuel synthesis is rationalized over a catalyst consisting 'C', 'Na', and 'Fe', as in NaFe@C, configured with ZSM-22 and ZSM-5 in CO_2 hydrogenation. While the 'Na' and 'C' functioned as structural promoters on Fe to enhance CO_2 conversion and olefins synthesis, the characteristics of the zeolites facilitated oligomerization of lighter hydrocarbons. A high $C_5 +$ selectivity was obtained over the HZSM-22 composite in CO_2 hydrogenation dominated by olefins and isoparaffins. Model reactions for exemplar oligomerization activity over the zeolites revealed ZSM-5 as highly active with selectivity towards isoparaffins and aromatic. The 'Na' cations induce Lewis's acid sites (LAS) which suppresses hydrocracking during chain growth. This consistency, revealed between the model and CO_2 hydrogenation unlocks a door to zeolite usage in CO_2 hydrogenation to clean heavy hydrocarbons.

1. Introduction

Zeolites can generally be defined as porous crystalline materials with well-defined pore and channel systems unique for applications in catalysis, separation, ion exchange, and adsorption [1–5]. They can highly be recognized in the heterogeneous catalysis sector, more specifically among hydrogenation processes mainly due to their amphiprotic nature, thermal stability, surface area, and their selective catalytic ability [6–8]. The CO_2 hydrogenation reaction can currently be recognized among processes expected to sufficiently exploit the characteristics of zeolites [9–13]. Concerns following the excessive dependence on fossil fuel resources have escalated thus intense attention has been drawn to the search for clean and sustainable options [14,15]. The CO_2 hydrogenation reaction has emerged as one of the rational routes to curb these climate concerns whiles doubling as a renewable option for the production of some valued hydrocarbons and oxygenates [16–19]. While the potential of this process remains large, progress has been limited to low-carbon chemicals and unstandardized liquid fuels mainly due to inadequate knowledge of catalytic systems with high C-C coupling mechanisms [20,21].

Heavy hydrocarbons ($C_5 +$) synthesis directly from CO_2 hydrogenation has been reported by just a handful [22,23]. Catalyst systems

effective for the reduction of CO_2 gas with a follow-up activity in high C-C chain growth to heavy hydrocarbon remain a paramount challenge. Moreover, specific catalyst structures for improved hydrocarbon species are sparse. As reported, excess aromatics in a fuel blend can produce more CO_2 emissions after combustion with the production of more ozone potential gases [24]. Thus fuels with substitute octane blends such as isoparaffins and low molecular olefins can be interesting options. While the popular catalytic approach involves the promotion of tailored Fe-based with alkali metals, the hydrocarbon distribution still follows the ASF model with limited selectivity to heavy hydrocarbons. Some multi-purpose composites, normally including two transitional metals have excelled in increasing the chain growth probability with outstanding selectivity towards heavy hydrocarbons [25–27]. A recent work by Yao et al. prepared a Fe-Mn-K composite catalyst by an organic combustion method for direct jet fuel synthesis from CO_2 hydrogenation. The 'Mn' and 'K' components do not function independently for CO_2 conversion or subsequent transformation of intermediates, they rather alter the intrinsic properties of the Fe phases into Fe species that orient the reaction to heavy hydrocarbons [28]. Alternative approach being employed consists of catalyst systems with distinct active materials. The metallic phases can be supported on popular high-surface materials such as SiO_2, Al_2O_3, and carbon. These materials can
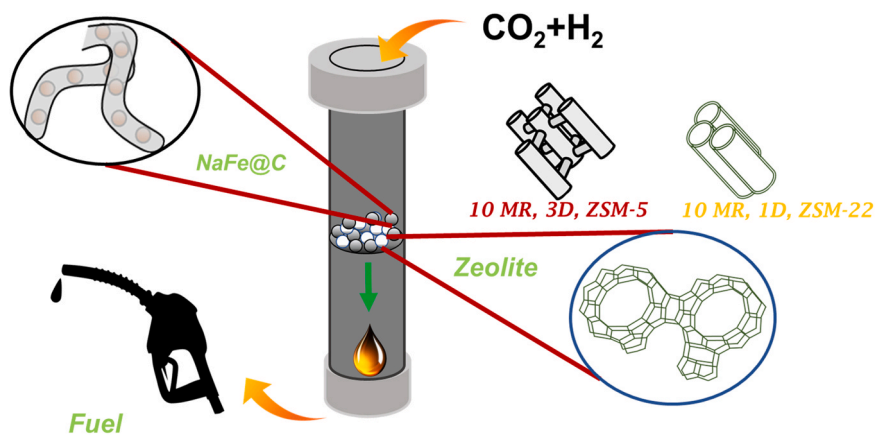
Fig. 1. Schematic for liquid fuel synthesis directly from CO_2 Hydrogenation.

improve the adsorption of CO_2 which is key for chain growth. The interest in carbon arises from their good thermal and chemical stability aside their superiority in improving the dispersion of the metallic phases as well as improve the selectivity for olefins [29]. In recent work, a thorough investigation was made on the influence of Fe-carbon composite with different synergistic effects in CO_2 hydrogenation [30]. The results indicated that encapsulating Fe in C facilitates the formation of more heavy hydrocarbons.

Subsequent activities within this domain have mostly employed metal composite catalyst with solid granules of zeolites to enhanced the selectivity for liquid hydrocarbons [12,22,31]. Consistent deductions suggest that zeolites mainly performed hydroprocessing functions on light hydrocarbons, mainly on the olefins. Also, the shape selective ability offered by the unique channel system and acid distributions determine the choice of zeolite for specific product selectivity [6,10,21, 32,32,33]. Results from various studies on Fe-zeolite composites indicate that Fe-based catalysts can produce ample amounts of olefins as intermediates for subsequent activities on the zeolites in CO_2 hydrogenation. Referencing a few literatures, conclusions can be drawn that MOR, SAPO-34, Beta, ZSM-58, and Y demonstrate hydrocracking reactions on heavy hydrocarbons to produce light hydrocarbons. Conversely, ZSM-22 and ZSM-5 both possessing 10 MR structures demonstrate oligomerization ability for heavy hydrocarbon production. Additionally, the different cation phases can alter the acid distribution of the zeolite which can be fully exploited by optimized reaction conditions [34]. ZSM-22 has been identified to be more biased towards heavy olefinic and isoparaffins products [10] while ZSM-5 influenced the selective production of cyclic, aromatics and branched products [21,33]. However, research limitations following details on the catalyst configurations and insight on chain growth mechanisms has necessitated performance of more investigations to reveal the zeolite configurations that enhance heavy hydrocarbon production directly in CO_2 hydrogenation.

Herein, we rationally perform experiments to increase heavy hydrocarbons directly in CO_2 hydrogenation using an NaFe@C catalysts coupled with ZSM-5 and ZSM-22 zeolites as shown in Fig. 1. The NaFe@C functions for olefin production by reducing CO_2 and facilitating subsequent hydrogenation to olefins. The olefins intermediate the formations of more heavy hydrocarbons over zeolite ZSM-5 and ZSM-22 in varying configurations. The results are interpreted on the basis of product distribution and main catalyst characteristics.

2. Experimental

2.1. Materials

$NaNO_3$ and NaOH, (Tianjin Kermel Chemical Reagent Company),

$C_{15}H_{21}FeO_6$ (Aladdin Industrial Corporation), Fe_3O_4 (10-20 nm, Shanghai Pantian Powder Co., Ltd.,)Multiwalled Carbon Nanotubes (MWCNT, Kaisa Guangdong New Materials Co., Ltd.), H-ZSM-22 zeolite, (Shanghai Aladdin Biochemical technology Co. Ltd), AlOOH (Xuan Cheng Jing Rui New materials Co. Ltd.), LUDOX AS-40 (Silica Sol, Sigma Aldrich), Tetra propylammonium hydroxide (TPAOH, Sinopharm Chemical Co. Ltd.), NH_4NO_3, and deionized water were used as chemical materials for the experiments. The as-obtained H-ZSM-22 and Fe_3O_4 were calcined in a muffle furnace for 3 h at 450 °C prior to use. All other materials were used as obtained without further purification steps.

2.2. Catalysts preparation

NaFe was prepared by impregnating 7.41 g $NaNO_3$ aqueous solution on 10 g of pre-treated Fe_3O_4 sample. The precursor was dried and calcined in air at 450 ^{0}C for 3 h. NaFe@C sample was prepared by simultaneous impregnation of solutions containing 7.097 g of $C_{15}H_{21}FeO_6$ and 3.44 g of $NaNO_3$ on 0.5 g of MWCNT. The precursor was dried and calcined in N_2 at 450 °C for 3 h. Details on the NaFe@C catalyst characterization can be seen in the supporting information. ZSM-5 with SiO_2/Al_2O_3 of 16 was prepared by adding 2 g of TPAOH to a solution containing measured quantities of NaOH and ALOOH. After stirring for a few minutes' silica sol was added to the solution and stirred thoroughly for 2 h. The mixture was transferred to a Teflon-lined autoclave and crystallized at 180 °C for 3 days. After cooling, the sample was washed, dried and calcined at 450 °C for 3 h to obtain NaZSM-5. The HZSM-5 sample was obtained from the prepared NaZSM-5 by ion exchange method using 0.5 M NH_4NO_3 solution at 70 °C for 1 h. The exchanged was performed twice. Subsequently, the sample was dried and calcined at 450 °C for 3 h. The as-obtained H-ZSM-22 zeolite was calcined in air at 450 °C for 3 h. NaZSM-22 zeolite was synthesized by treating as obtained H-ZSM-22 with 0.5 molar $NaNO_3$ solution at 70 °C for 1 h. The solution was exchanged twice to ensure enough ion exchange. Subsequently, the samples were dried and calcined at 450 °C for 3 h.

2.3. Catalyst characterization

CO_2-TPD of catalysts was achieved on a Microtrac Belcat II. In a typical procedure, 0.05 g of each catalyst was loaded and reduced in H_2 for 4 h. The sample were allowed to cool and CO_2/He= 6:5.03% was introduced for 30 mins. The adsorbed gas was degassed in He from 100 to 900 °C. X-ray Diffractograms (XRD) patterns of the catalysts were achieved on PANALytical Xpert Pro diffractometer having Cu Kα radiation at 40 A, and 40 V. N_2-physisorption on an Autosorb-iQ instrument (Quantachrome Co., Ltd.) was used to attain the textural properties of the catalysts. In a typical process, a mass of 0.2 g for each sample was
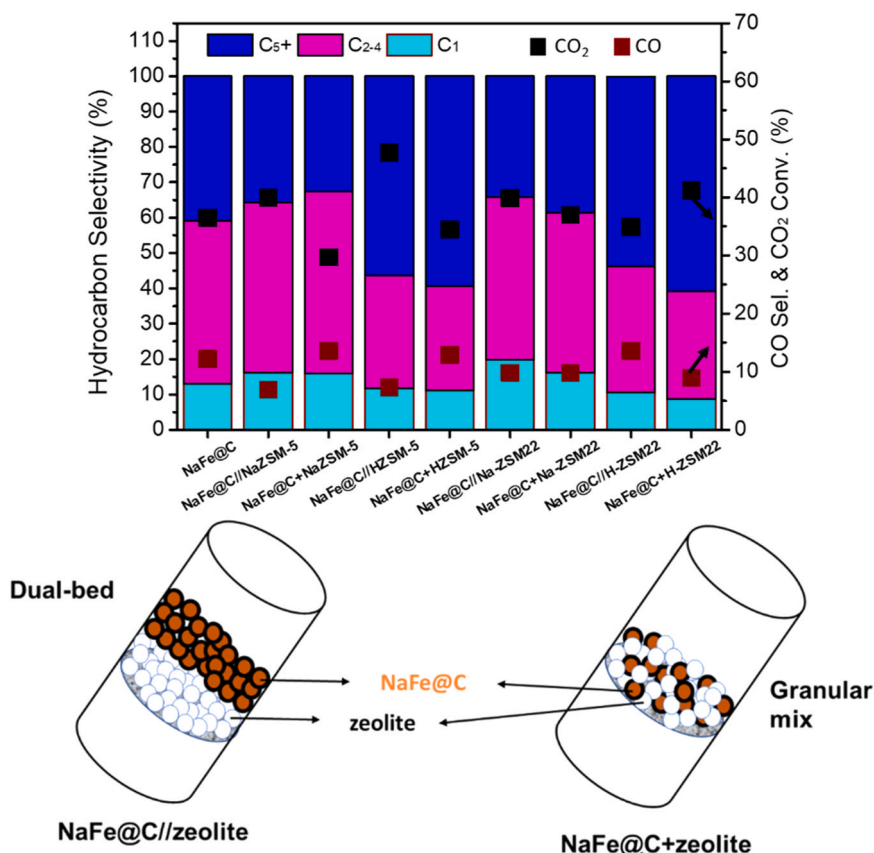
Fig. 2. Catalyst Activity and Product Distribution of the catalysts. ***GHSV***= 4000 mL·h^{-1}·g^{-1}, ***Pressure*** = 3 MPa, ***Temperature*** = 300 °C.

used in this process. The samples were first degassed at 300 °C for 3 h to remove undesired organics, gases, and water. The surface area was calculated from the Brunauer-Emmett- Teller (BET) equation and pore volume from the Barrett-Joyner-Halenda (BJH). X-ray photoelectron spectroscopy (XPS) used to qualitatively and quantitatively analyze the nature of the surface elements was obtained on a Thermo ESCALAB 250XI spectrometer. H$_2$-Temperature Programmed Reduction (H$_2$-TPR) of the catalysts were obtained on a Microtrac Belcat II. In a typical procedure, the samples were initially degassed in Ar at 350 °C for 1 h. The sample were cooled down and 4:5 =H$_2$/Ar gas was introduced as temperature was raised from 30 to 900 °C at a ramp rate of 10 °C. Raman spectra were measured using a Jobin-Yvon T64000 with a spectral resolution of 2 cm^{-1}. Fourier transform infrared (FT-IR) spectroscopy of the samples was conducted over a Bruker V70 IR spectrometer. XRF of the zeolites was conducted on Paneko Zetium. Pyridine-IR (PY-IR) was achieved on an FTIR-650 FT-IR spectrometer to qualitatively analyze the acidity of the zeolite catalysts. The samples were prepared on a thin wafer and pre-treated at 450 °C in a vacuum. The prepared slides were then cooled down to room temperature, exposed to pyridine for 5 mins and then finally evacuated at 150 and 350 °C for 30 min. NH$_3$ temperature-programmed desorption (NH$_3$-TPD) of the samples was also carried out on a BELCAT-B3 instrument equipped with a TCD. The samples were first pretreated in pure He at a flow rate and a temperature of 30 mL min^{-1} and 300 °C, respectively. Thereafter, the equipment was cooled, and gas with NH$_3$/He = 5/95 at a flow rate of 20 mL min^{-1} was introduced as the temperature was raised from 100 to 700 °C, at a heating rate of 10 °C min^{-1}. Scanning Electron Microscopy (SEM) images were taken on a Hitachi Regulus8100. NMR was achieved with a Bruker AVWBIII600. The NMR was achieved with a 4 mm probe at a spin rate of 12 kHz for ^{13}C CPMAS and 14 kHz for both ^{1}H MAS and ^{27}Al MAS NMR. The spin rate for was ^{29}Si MAS NMR was 10KHz.

2.4. CO$_2$ hydrogenation reactions

The activities of the catalysts in the CO$_2$ hydrogenation reaction were evaluated using a single fixed-bed reactor under 300 °C, H$_2$/CO$_2$ = 3/1, and with Flowrate = 20 mL/min. For each reaction, measured mass of catalyst as indicated is mixed with 1 g of quarts and loaded in a continuous flow stainless steel reactor and reduced at 360 ∘C for 8 h in H$_2$ flow (40 mL/min). The reactor was allowed to cool reaction temperature while the reaction gas is being introduced to raised pressure to required pressure as indicated below each distribution. The reaction began when the temperature and pressure reach their set conditions. Two online gas chromatographs (TCD and FID) were used to analyze the effluent gaseous products. The TCD and FID were equipped with an Agilent HP-Plot/Q column and a PONA column respectively. Some liquid products were collected in an ice trap and later analyzed offline by the FID gas chromatograph. Catalyst activity and product selectivity were calculated on a molar basis.

$$CO_2 \quad conversion(\%) = \frac{F_{CO_{2(in)}} - F_{CO_{2(out)}}}{F_{CO_{2(in)}}} \times 100 \qquad (1)$$

Where; $F_{CO_{2(in)}} = inlet \quad CO_2 \quad molar \quad flow$

$F_{CO_{2(out)}} = outlet \quad CO_2, molar \quad flow$

$$Hydrocarbon \quad Selectivity \quad (\%) = \frac{nF_{c_{n(out)}}}{F_{CO_{2(in)}} - F_{CO_{2(out)}}} \times 100 \qquad (2)$$

Where; $C_n = carbon \quad number \quad of \quad product$

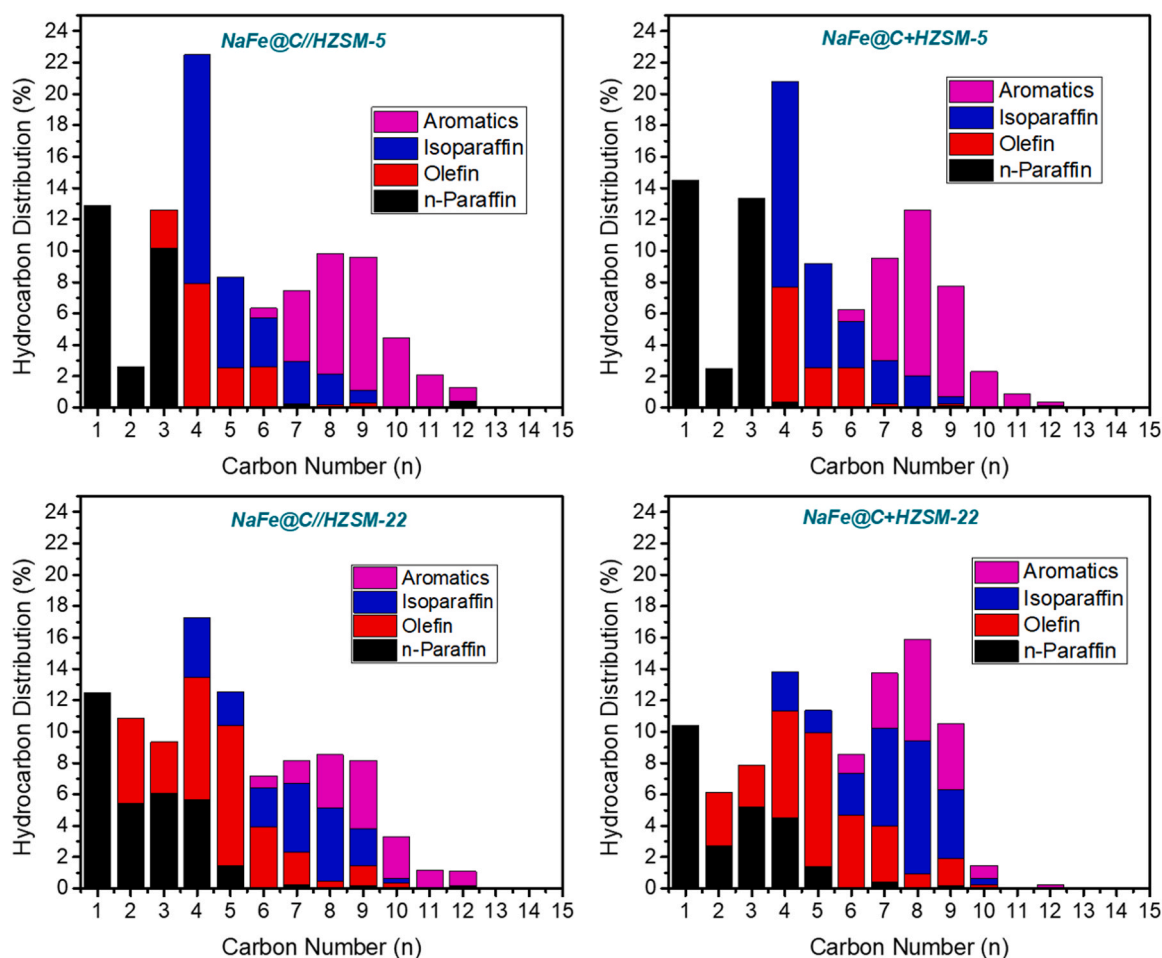$F_{c_{n(out)}} = outlet \quad molar \quad flowrate \quad of \quad product \quad C_n$

Fig. 3. The hydrocarbon product distribution associated with the NaFe@C coupled with the H-type zeolites.

2.5. Olefins oligomerization reactions

The oligomerization tests of the zeolites were carried out in a fixed-bed reactor using a gas mixture of $C_2H_4/C_3H_8/Ar$ with a ratio of 10.01/5.01/84.98. In a typical procedure, 0.3 g of each zeolite catalyst was loaded into reactor after which temperature and pressure were raised to 300 °C and 3 MPa, respectively to begin the reaction with a flowrate of 20 mL/min. The effluents were analyzed both online and offline by a gas chromatograph equipped with an FID. The FID was operated with a PONA column. The liquid products were collected in an ice trap and later analyzed offline by the FID gas chromatograph. Catalyst activity and product selectivity were calculated on a molar basis.

$$C_nH_y \, conversion(\%) \frac{F_{C_nH_{y(in)}} - F_{C_nH_{y(out)}}}{F_{C_nH_{y(in)}}} \times 100 \qquad (3)$$

Where; $F_{C_nH_{y(in)}} = inlet \ molar \ flow \ of \ specific \ olefin$

$F_{C_nH_{y(out)}} = outlet \ molar \ flow \ of \ specific \ olefin$

$$Hydrocarbon \quad Selectivity(\%) = \frac{nF_{c_{n(out)}}}{F_{C_nH_{y(in)}} - F_{C_nH_{y(out)}}} \times 100 \qquad (4)$$

Where; $C_n = carbon \ number \ of \ product$

$F_{c_{n(out)}} = outlet \ molar \ flowrate \ of \ product \ C_n$

3. Results and discussion

3.1. Catalyst activity

3.1.1. CO₂ hydrogenation

The Figs. 2 and 3 displays results for CO_2 hydrogenation reactions over NaFe@C catalyst and NaFe@C coupled with zeolites as well as the carbon number associated with the different product distributions. From literature, a combination of carbon and alkali-promoted Fe-based catalysts normally results in improved selectivity for long chain hydrocarbons and olefins in the final product. This is proved by comparing the activities between the NaFe and NaFe@C as demonstrated in the Table S1. The carbon favors the production of more heavy hydrocarbons. The NaFe@C catalyst demonstrates a selectivity of ~40.9% for C_5 + hydrocarbons. The total olefins recorded was 59% with 30% being light olefins in products. Nevertheless, the distribution is limited to the ASF model, thus a retrained selectivity for heavy hydrocarbons is observed [35].

To further improve the selectivity for heavy hydrocarbons, the zeolites ZSM-22 and ZSM-5 in 'Na' and 'H' forms are further coupled with NaFe@C in dual bed and granular mix mode as presented in Figs. 2 and 3, and Table S1. All 'H' forms of the zeolites contribute to chain growth, raising the C_5 + selectivity from 40.9% over the NaFe@C catalyst to over 53% over the least performing H-type zeolite. The products over H-ZSM-5 were dominated by isoparaffins and aromatics, whereas over HZSM-22 was dominated by heavy olefins and isoparaffins. Limited activity was observed over the Na-types with reduced selectivity to C_5 + hydrocarbons. The general conclusion drawn from these results is that
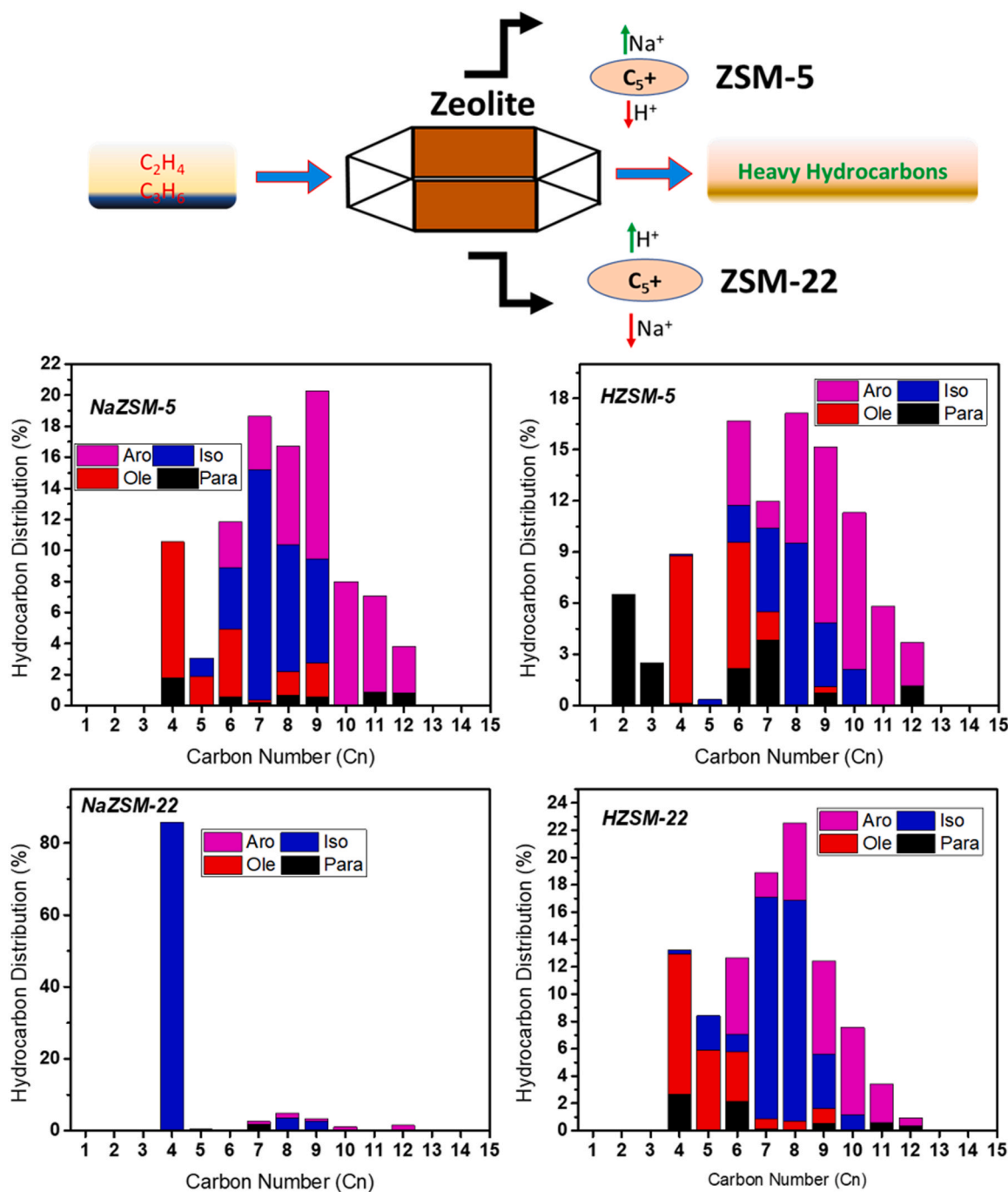
Fig. 4. **(a)** Schematic representing oligomerization over the different zeolites. **(b)** C_2H_4, C_3H_6 oligomerization over zeolites. G*HSV*= 4000 mL·h^{-1}·g^{-1}, ***Pressure*** = 3 MPa, ***Temperature*** = 300 °C.

oligomerization in CO_2 hydrogenation is high over the proton forms of the zeolites and are more active when the two catalysts are distinct and in close proximity. The distinct features of the NaFe@C catalyst (Fig. S1, S2 and S3) functions for efficient production of olefins which are transformed as intermediates on the zeolites. The different structures of the zeolites define the type of hydrocarbons produced

3.1.2. Oligomerization

Oligomerization is the fundamental function of zeolites exploited in this work. A feed gas comprising 10%C_2H_4, and 5%C_3H_6 is used to investigate the oligomerization of light hydrocarbons over the zeolites to better comprehend their oligomerization activity in CO_2 hydrogenation. Olefins are enhanced in their adsorption capacity over alkanes on

zeolites as they are adsorbed closer to the zeolite wall where they are subsequently chemisorbed by interactions with the cation [36]. Thus the zeolites in CO_2 hydrogenation hold higher propensity to oligomerize if the feed comprises ample concentration of olefins [37–39]. As shown in Table S2 and Fig. 4, a high olefins conversion was realized on the H-type zeolites (HZSM-5 &HZSM-22) with HZSM-5 demonstrating the most conversion of ~91.3 & 97.8% for C_2H_4 and C_3H_6, respectively. This indicates that the protons forms of the zeolites are more active in hydroprocessing. NaZSM-5 performed better for olefins conversion when compared with NaZSM-22. This suggests irrespective of the cation present, the MFI topology possesses characteristics that enhance the conversion of olefins over their corresponding TON. A higher selectivity for C_5 + hydrocarbons is recorded for NaZSM-5 over HZSM-5 zeolite in
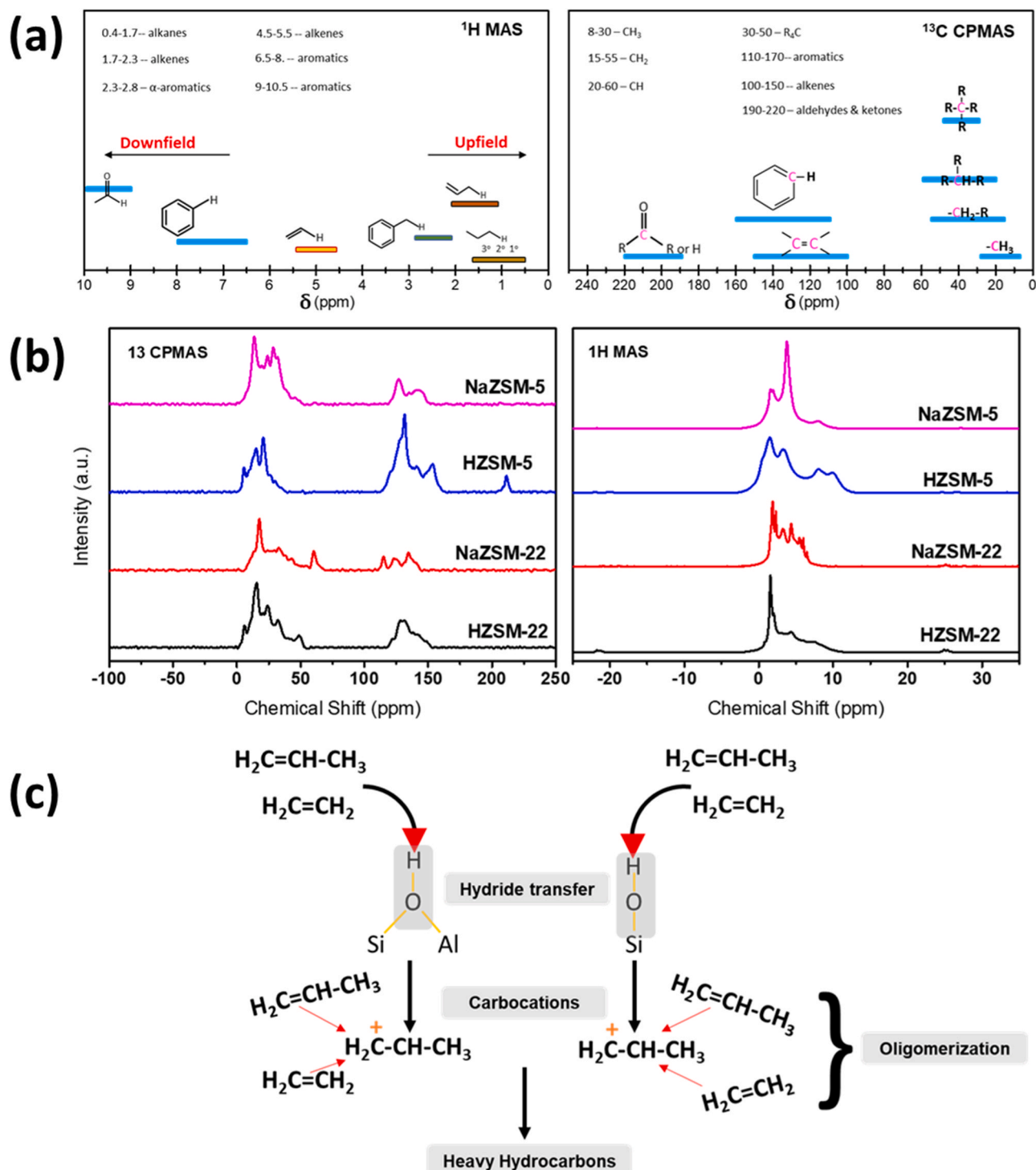
Fig. 5. ^1H and ^{13}C NMR spectroscopy of the spent zeolite catalyst.

addition to reduced selectivity for paraffins in the final products. This suggests that 'Na' on ZSM-5 assumes properties, promoting hydrocarbon chain growth over 'H' on ZSM-5. Conversely, a higher selectivity of C_5 + hydrocarbons is recorded for HZSM-22 over NaZSM-22 zeolite. This indicates that the activity of the cations in oligomerization are hugely impacted by the framework topology. Results from the oligomerization activity can well translate the effects of zeolites in CO_2 hydrogenation. From the olefin model reactions, the highest olefin conversion and oligomerization activity was recorded over the H-type zeolites which is similarly recorded during the CO_2 hydrogenation activity. The

selectivity for isoparaffins is higher over both ZSM-22 zeolites during the olefin oligomerization, however lower than ZSM-5 in CO_2 hydrogenation. It has been suggested from the literature that the topology of ZSM-22 is favorable for the skeletal isomerization reactions of olefins, nevertheless, the oligomerization activity of HZSM-5 is generally higher in CO_2 hydrogenation which probably leads to higher isoparaffins in the final product [40]. Additionally, heavy olefins are improved over HZSM-22 which is synonymous with the results from CO_2 hydrogenation. This confirms that the 1-D structures of HZSM-22 are favorable for linear chain growth for higher olefins and light branching for
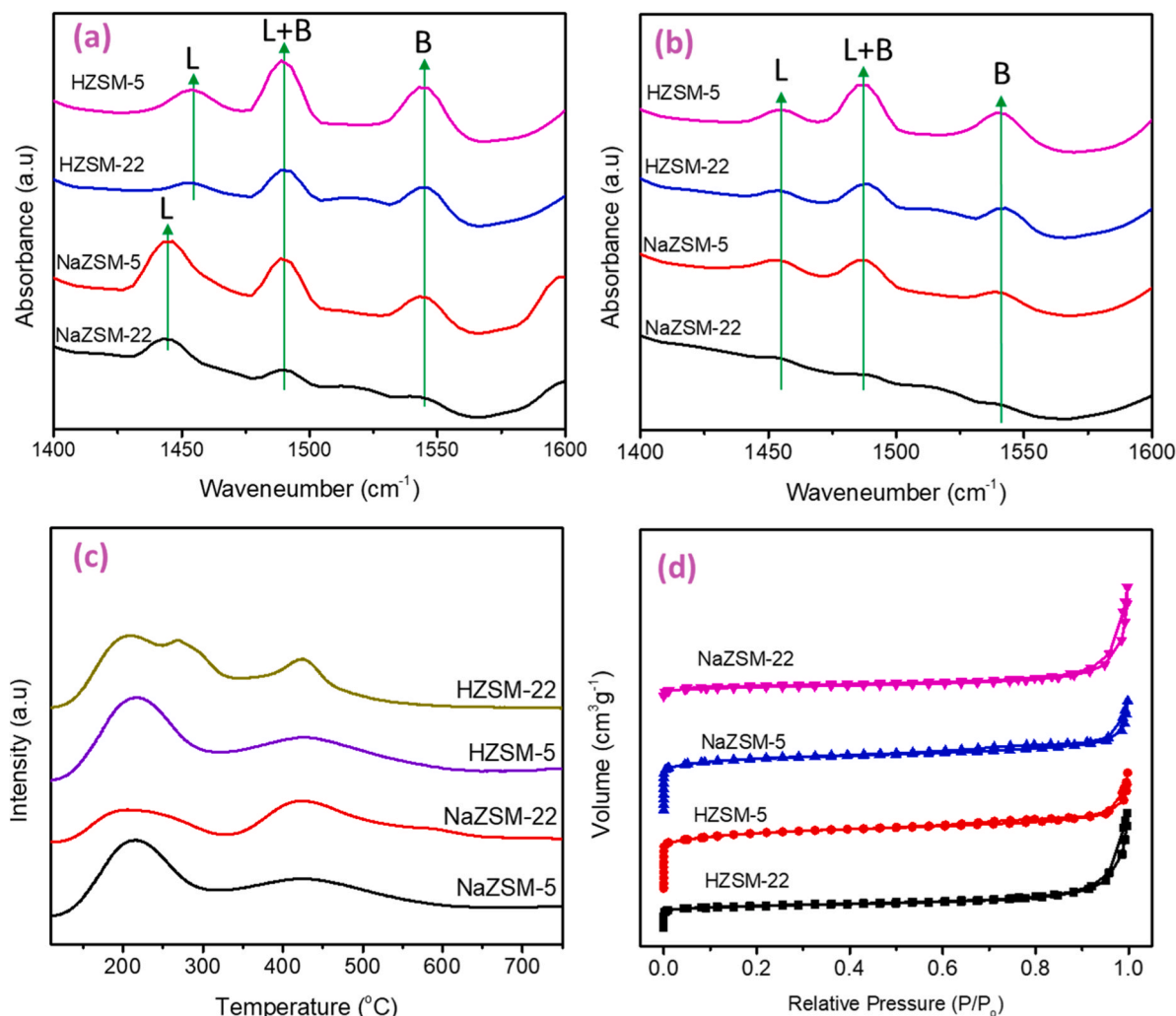
Fig. 6. Acidity (a-c) and Pore properties of the zeolite catalysts (a) 150 °C, and (b) 350 °C, (c) NH$_3$-TPD, (d) N$_2$-physisorption isotherms.

isoparaffins. Selectivity as demonstrated by ZSM-5 results in the formation of more branched hydrocarbons and aromatics. This equally corresponds to the results recorded earlier from CO$_2$ hydrogenation. The 3-D channel system of the MFI facilitated the aromatization and isomerization of the primary hydrocarbons.

3.2. Catalyst characterizations

3.2.1. NMR

^{13}C and ^{1}H NMR analysis is done on the spent zeolites after oligomerization to confirm and predict dominating products and intermediates that follow the activity of the zeolite after olefin oligomerization. Peaks observed from the ^{13}C NMR shifts of 18, 135, 116, and 123 ppm and the ^{1}H shifts of 1.55 and 5.45–5.55 represents terminal -CH$_3$ and -C=C- which can identify the adsorbed C$_2$H$_4$ and C$_3$H$_6$ reactants on the surfaces of the zeolites. A glance at the peak obtained from the ^{13}C NMR spectrum reveals lower peak intensities for the NaZSM-22 profile which suggests a low quantity of adsorbed species also suggesting low activity. This is further confirmed by the conversely strong peak intensities for the adsorbed C$_2$H$_4$ and C$_3$H$_6$ dominating among the other zeolites catalysts indicating much higher activity. Nevertheless, notable peaks can be identified around 135 ppm for the ^{13}C spectrum corresponded with 4.5–6.5 ppm from the ^{1}H spectrum suggests bonds associated with some heavier olefins and aromatics.

Aside that, the other zeolites demonstrate higher intensities for other species suggesting significant oligomerization activity. High peak intensities recorded between 100 and 150 ppm for NaZSM-5 and HZSM-5 can be assigned to double bonded and aromatic hydrocarbon species which suggests the formation of more heavy olefins and aromatics during oligomerization. This is supported by the ^{1}H peak recorded at 7.8–9.9 ppm which represents C-H bonded in aromatic rings. The key difference observed between the two ZSM-5 zeolites is that a single peak at ~7.7 ppm for NaZSM-5 ascribed to C-H bonds associated with mono-aromatics whereas a twin peak ascribed to both mono-, and poly-aromatics are well recognized on the surfaces of HZSM-5. H-ZSM-22 demonstrates peaks to indicate the formation of more alkanes, mono-aromatic, and olefins. More peaks are fitted between 0 and 30 ppm of the ^{13}C spectrum to suggest the dominating presence of alkanes. All zeolites show peaks representing alkoxides and hydroxyl groups which represent the stages of adsorption and intermediate transformation. These results can project the reaction steps involved in the oligomerization process. Primarily, the olefins are initially adsorbed on the zeolite surface where they bond and displace the cation as demonstrated in the scheme below and Fig. S7. The reaction proceeds mostly with bonds to the protons on the H-type zeolite whereas the silanol groups mainly define alkoxide formation on the Na-type zeolite. As seen from the scheme, a series of hydride transfers leads to the formation of unstable carbenium ion which easily reacts with other olefins for chain propagation. The carbenium ion easily undergoes skeletal rearrangement to form branched species. The formation of aromatics is mostly structurally defined with respect to the zeolite topology. This has limited their formation over the 1-D channels of ZSM-22. Aromatics formation is

dominant over the 3-D structures of ZSM-5. Fig. 5.

3.2.2. Physical and chemical characteristics

The acid and pore properties of the zeolites are presented in Fig. 6. While the XRF characterization from Table S3 suggest the SiO_2/Al_2O_3 ratio of the ZSM-22 is about twice that of ZSM-5, the NH_3-TPD profile reveals profiles with intensities almost similar for the as-obtained proton forms. Two main peaks are identified for all samples. The peak appearing between ~150–300 °C and ~350–600 °C represents weak acid and strong acid sites, respectively. The acidity is seen to reduce over 'Na$^+$' type zeolites. Under same conditions, a reduction in peak intensity occurs more over NaZSM-22 than NaZSM-5. Further analysis of the acidity in terms of quality and quantity was further revealed by Py-IR. Both Lewis acid sites (LAS) and Brønsted acid sites (BAS) were identified in all zeolite samples. Analysis from the numerical data in Table S4 suggests that the H-type zeolites demonstrate high BAS. However, for the Na-type, the BAS sites are reduced which corresponded to an increase in the LAS, induced by the Na ions. Comparing by variations in the temperature, conclusions can be drawn that the ion exchange leads to an increase in BAS over the H-type zeolites. Relating the acidity to the product distribution suggests that generally, the presence of more acid sites facilitates hydroprocessing activities with oligomerization being prominent. Referencing the results from the oligomerization model reveal that BAS is advantageous for hydroprocessing, however, excess can limit the chain propagation with significant activity in hydrocracking. This is confirmed by comparing the oligomerization results between NaZSM-5 and HZSM-5. Higher olefin conversions are achieved over HZSM-5 however limited in oligomerization to NaZSM-5. Furthermore, the differences in distribution can clearly be translated as a result of the different structures and pore geometry following the zeolites. The Fig. S4-7, and Table S6 summarizes the characteristics of the zeolites. The highest BET surface area is realized on both ZSM-5 samples. This may be confirming an advantageous structural characteristic of ZSM-5 as hypothesized earlier. The 'Na' forms of the different zeolites demonstrated reduced surface area but approximately maintained the pore volumes.

4. Conclusions

In summary, this work has rationalized the synthesis of liquid fuels over NaFe@C and zeolite composite. The focus is placed on the influential factors accompanying the catalyst characteristics. The NaFe@C functioned for CO_2 conversion and olefins production. The olefins were subsequently converted to heavy hydrocarbons over zeolites. Key revelations from this work indicates that while hydroprocessing is high with increasing acid sites, oligomerization and product selectivity are defined by the zeolite topology. Combined NMR and acid characterizations reveal that medium and weak acid sites are advantageous for oligomerization of light olefins to more monoaromatic compounds. The MFI topology demonstrated higher selectivity for aromatics and isoparaffins whereas HZSM-22 demonstrates higher activity for heavy olefins, monoaromatics and isoparaffins. Highest heavy hydrocarbons selectivity was achieved when NaFe@C was coupled with HZSM-22 in granular mix mode. The products were dominated by isoparaffins and olefins.

CRediT authorship contribution statement

Cederick Cyril Amoo: Conceptualization, Writing – original draft, Methodology. **Joshua Iseoluwa Orege:** Writing – review & editing, Methodology. **Qingjie G:** Supervision, Conceptualization. **Jian Sun:** Supervision, Conceptualization.

Declaration of Competing Interest

The authors declare that they have no competing financial interests

or personal relationships that could appeared to influence the work reported in this paper.

Data Availability

Data will be made available on request.

Appendix A. Supporting information

Supplementary data associated with this article can be found in the online version at doi:10.1016/j.apcatb.2023.123193.

References

[1] Q. Zhang, S. Gao, J. Yu, Metal sites in zeolites: synthesis, characterization, and catalysis, Chem. Rev. (2022).

[2] G. Fu, E. Dib, Q. Lang, H. Zhao, S. Wang, R. Ding, X. Yang, V. Valtchev, Acidic medium synthesis of zeolites – an avenue to control the structure-directing power of organic templates, Dalton Trans. 51 (30) (2022) 11499–11506.

[3] Shape-Selective Catalysis: Zeolites. In *Industrial Catalysis*, 2005; pp 239–259.

[4] R. Barakov, N. Shcherban, P. Mäki-Arvela, P. Yaremov, I. Bezverkhyy, J. Wärnå, D. Y. Murzin, Hierarchical Beta Zeolites As catalysts in α-pinene oxide isomerization, ACS Sustain. Chem. Eng. 10 (20) (2022) 6642–6656.

[5] M. Dusselier, M.E. Davis, Small-pore zeolites: synthesis and catalysis, Chem. Rev. 118 (11) (2018) 5265–5329.

[6] C.C. Amoo, C. Xing, N. Tsubaki, J. Sun, Tandem reactions over zeolite-based catalysts in syngas conversion, ACS Cent. Sci. 8 (8) (2022) 1047–1062.

[7] J. Hajek, B. Bueken, M. Waroquier, D. DeVos, V. VanSpeybroeck, The remarkable amphoteric nature of defective UiO-66 in catalytic reactions, ChemCatChem 9 (12) (2017) 2203–2210.

[8] S. Navarro-Jaén, M. Virginie, J. Bonin, M. Robert, R. Wojcieszak, A.Y. Khodakov, Highlights and challenges in the selective reduction of carbon dioxide to methanol, Nat. Rev. Chem. 5 (8) (2021) 564–579.

[9] B. Chan, L. Radom, Zeolite-catalyzed hydrogenation of carbon dioxide and ethene, J. Am. Chem. Soc. 130 (30) (2008) 9790–9799.

[10] A. Ramirez, X. Gong, M. Caglayan, S.-A.F. Nastase, E. Abou-Hamad, L. Gevers, L. Cavallo, A. Dutta Chowdhury, J. Gascon, Selectivity descriptors for the direct hydrogenation of CO_2 to hydrocarbons during zeolite-mediated bifunctional catalysis, Nat. Commun. 12 (1) (2021) 5914.

[11] I. Graça, L.V. González, M.C. Bacariza, A. Fernandes, C. Henriques, J.M. Lopes, M. F. Ribeiro, CO_2 hydrogenation into CH_4 on NiHNaUSY zeolites, Appl. Catal. B: Environ. 147 (2014) 101–110.

[12] J. Zhang, M. Zhang, S. Chen, X. Wang, Z. Zhou, Y. Wu, T. Zhang, G. Yang, Y. Han, Y. Tan, Hydrogenation of CO_2 into aromatics over a ZnCrOx–zeolite composite catalyst, Chem. Commun. 55 (7) (2019) 973–976.

[13] L. Wang, Y. Han, J. Wei, Q. Ge, S. Lu, Y. Mao, J. Sun, Dynamic confinement catalysis in Fe-based CO_2 hydrogenation to light olefins, Appl. Catal. B: Environ. 328 (2023), 122506.

[14] Y. Fu, C.C. Amoo, H. Qi, H. Liu, L. Zhu, P. Lu, R. Yang, C. Xing, S. Wang, J. Sun, EDTA chemical directly orient CO_2 hydrogenation towards olefins, Chem. Eng. J. 438 (2022) 135597.

[15] N. Liu, J. Wei, J. Xu, Y. Yu, J. Yu, Y. Han, K. Wang, J.I. Orege, Q. Ge, J. Sun, Elucidating the structural evolution of highly efficient Co–Fe bimetallic catalysts for the hydrogenation of CO_2 into olefins, Appl. Catal. B: Environ. 328 (2023), 122476.

[16] J. Zhou, Z. Gao, G. Xiang, T. Zhai, Z. Liu, W. Zhao, X. Liang, L. Wang, Interfacial compatibility critically controls Ru/TiO2 metal-support interaction modes in CO_2 hydrogenation, Nat. Commun. 13 (1) (2022) 327.

[17] S. Shao, C. Cui, Z. Tang, G. Li, Recent advances in metal-organic frameworks for catalytic CO_2 hydrogenation to diverse products, Nano Res. (2022).

[18] W. Gao, S. Liang, R. Wang, Q. Jiang, Y. Zhang, Q. Zheng, B. Xie, C.Y. Toe, X. Zhu, J. Wang, L. Huang, Y. Gao, Z. Wang, C. Jo, Q. Wang, L. Wang, Y. Liu, B. Louis, J. Scott, A.-C. Roger, R. Amal, H. He, S.-E. Park, Industrial carbon dioxide capture and utilization: state of the art and future challenges, Chem. Soc. Rev. 49 (23) (2020) 8584–8686.

[19] C. Meng, G. Zhao, X.-R. Shi, Q. Nie, Y. Liu, Y. Lu, Electronic modulation of InNi3C0.5/Fe3O4 by support precursor toward efficient CO_2 hydrogenation to methanol, Appl. Catal. B: Environ. 316 (2022), 121699.

[20] A. Ramirez, A. Dutta Chowdhury, A. Dokania, P. Cnudde, M. Caglayan, I. Yarulina, E. Abou-Hamad, L. Gevers, S. Ould-Chikh, K. De Wispelaere, V. van Speybroeck,

J. Gascon, Effect of zeolite topology and reactor configuration on the direct conversion of CO$_2$ to light olefins and aromatics, ACS Catal. 9 (7) (2019) 6320–6334.

[21] A. Noreen, M. Li, Y. Fu, C.C. Amoo, J. Wang, E. Maturura, C. Du, R. Yang, C. Xing, J. Sun, One-pass hydrogenation of CO$_2$ to multibranched isoparaffins over bifunctional zeolite-based catalysts, ACS Catal. 10 (23) (2020) 14186–14194.

[22] J. Wei, R. Yao, Y. Han, Q. Ge, J. Sun, Towards the development of the emerging process of CO$_2$ heterogenous hydrogenation into high-value unsaturated heavy hydrocarbons, Chem. Soc. Rev. 50 (19) (2021) 10764–10805.

[23] L. Xiong, S. Liu, Y. Men, L. Li, X. Niu, K. Guo, J. Xu, W. An, J. Wang, Y. Cong, Highly selective hydrogenation of CO$_2$ to C5+ hydrocarbons over Fe catalysts copromoted by K with Pd, J. Environ. Chem. Eng. 10 (5) (2022) 108407.

[24] I. Schifter, L. Díaz, G. Sánchez-Reyna, C. González-Macías, U. González, R. Rodríguez, Influence of gasoline olefin and aromatic content on exhaust emissions of 15% ethanol blends, Fuel 265 (2020) 116950.

[25] L. Zhang, Y. Dang, X. Zhou, P. Gao, A. Petrus van Bavel, H. Wang, S. Li, L. Shi, Y. Yang, E.I. Vovk, Y. Gao, Y. Sun, Direct conversion of CO$_2$ to a jet fuel over CoFe alloy catalysts, *Innovation* 2 (4) (2021), 100170.

[26] P. Gao, L. Zhang, S. Li, Z. Zhou, Y. Sun, Novel Heterogeneous Catalysts for CO$_2$ hydrogenation to liquid fuels, ACS Cent. Sci. 6 (10) (2020) 1657–1670.

[27] Z. He, M. Cui, Q. Qian, J. Zhang, H. Liu, B. Han, Synthesis of liquid fuel via direct hydrogenation of CO$_2$, *Proc. Natl. Acad. Sci.* 116 (26) (2019) 12654–12659.

[28] B. Yao, T. Xiao, O.A. Makgae, X. Jie, S. Gonzalez-Cortes, S. Guan, A.I. Kirkland, J. R. Dilworth, H.A. Al-Megren, S.M. Alshihri, P.J. Dobson, G.P. Owen, J.M. Thomas, P.P. Edwards, Transforming carbon dioxide into jet fuel using an organic combustion-synthesized Fe-Mn-K catalyst, Nat. Commun. 11 (1) (2020) 6395.

[29] R.-P. Ye, J. Ding, W. Gong, M.D. Argyle, Q. Zhong, Y. Wang, C.K. Russell, Z. Xu, A. G. Russell, Q. Li, M. Fan, Y.-G. Yao, CO$_2$ hydrogenation to high-value products via heterogeneous catalysis, Nat. Commun. 10 (1) (2019) 5698.

[30] C.C. Amoo, J.I. Orege, Q. Ge, J. Sun, Exploiting the latency of carbon as catalyst in CO$_2$ hydrogenation, Chem. Eng. J. 471 (2023), 144606.

[31] X. Wang, G. Yang, J. Zhang, F. Song, Y. Wu, T. Zhang, Q. Zhang, N. Tsubaki, Y. Tan, Macroscopic assembly style of catalysts significantly determining their efficiency for converting CO$_2$ to gasoline, Catal. Sci. Technol. 9 (19) (2019) 5401–5412.

[32] J. Wei, Q. Ge, R. Yao, Z. Wen, C. Fang, L. Guo, H. Xu, J. Sun, Directly converting CO$_2$ into a gasoline fuel, Nat. Commun. 8 (1) (2017) 15174.

[33] C. Xing, M. Li, G. Zhang, A. Noreen, Y. Fu, M. Yao, C. Lu, X. Gao, R. Yang, C. C. Amoo, Syngas to isoparaffins: rationalizing selectivity over zeolites assisted by a predictive isomerization model, Fuel 285 (2021), 119233.

[34] L. Guo, S. Sun, J. Li, W. Gao, H. Zhao, B. Zhang, Y. He, P. Zhang, G. Yang, N. Tsubaki, Boosting liquid hydrocarbons selectivity from CO$_2$ hydrogenation by facilely tailoring surface acid properties of zeolite via a modified Fischer-Tropsch synthesis, Fuel 306 (2021), 121684.

[35] F.A. De la Rosa-Priego, E.D. Gutierrez-López, T.A. Zepeda, M. Acosta-Alejandro, A. M. Venezia, S. Fuentes-Moyado, B. Pawelec, J.N. Díaz-de-León, Enhanced CO$_2$ hydrogenation to C2+ hydrocarbons over mesoporous x%Fe2O3–Al2O3 Catalysts, Ind. Eng. Chem. Res. 60 (51) (2021) 18660–18671.

[36] B.A. De Moor, M.-F. Reyniers, G.B. Marin, Physisorption and chemisorption of alkanes and alkenes in H-FAU: a combined ab initio–statistical thermodynamics study, Phys. Chem. Chem. Phys. 11 (16) (2009) 2939–2958.

[37] S. Moon, H.-J. Chae, M.B. Park, Oligomerization of light olefins over ZSM-5 and beta zeolite catalysts by modifying textural properties, Appl. Catal. A: Gen. 553 (2018) 15–23.

[38] S. Vernuccio, E.E. Bickel, R. Gounder, L.J. Broadbelt, Microkinetic model of propylene oligomerization on brønsted acidic zeolites at low conversion, ACS Catal. 9 (10) (2019) 8996–9008.

[39] Y. Li, L. Zeng, G. Pang, X. Wei, M. Wang, K. Cheng, J. Kang, J.M. Serra, Q. Zhang, Y. Wang, Direct conversion of carbon dioxide into liquid fuels and chemicals by coupling green hydrogen at high temperature, Appl. Catal. B: Environ. 324 (2023), 122299.

[40] W. Li, K. Chi, H. Liu, H. Ma, W. Qu, C. Wang, G. Lv, Z. Tian, Skeletal isomerization of n-pentane: a comparative study on catalytic properties of Pt/WOx–ZrO2 and Pt/ZSM-22, Appl. Catal. A: Gen. 537 (2017) 59–65.